Power-law Fluid Flow around an Elliptical Cylinder in Laminar Flow Regime

Sidhartha Tirthankar

Department of Chemical Engineering
National Institute of Technology Rourkela

Power-law Fluid Flow around an Elliptical Cylinder in Laminar Flow Regime

Dissertation submitted to the

National Institute of Technology Rourkela

in partial fulfillment of the requirements

of the degree of

Bachelor of Technology

in

Chemical Engineering

by

Sidhartha Tirthankar

(Roll Number: 112CH0101)

under the supervision of

Prof. Akhilesh Kumar Sahu

May, 2016

Department of Chemical Engineering

National Institute of Technology Rourkela

Department of Chemical Engineering
National Institute of Technology Rourkela

Prof. Akhilesh Kumar Sahu

Assistant Professor

May 11, 2016

Supervisor's Certificate

This is to certify that the work presented in this dissertation entitled "*Power-law Fluid Flow around an Elliptical Cylinder in Laminar Flow Regime*" by "*Sidhartha Tirthankar*", Roll Number 112CH0101, is a record of original research carried out by him under my supervision and guidance in partial fulfillment of the requirements of the degree of *Bachelor of Technology* in *Chemical Engineering*.

Akhilesh Kumar Sahu

Acknowledgement

First, I would like to thank my project supervisor Prof. Akhilesh Kumar Sahu for the innumerable hours he put forth for ensuring that my project work and report is top-notch; his doors have always been open for me. I am immensely grateful to him for clearing all my doubts and ensuring that I write a proper scientific report. I have learnt a lot about how to approach a topic while doing research, how to survey the vast literature for the same and proceed in the right direction. His unwavering support throughout the term of my project has had an indelible effect on my life.

Second, I would like to thank Prof. Pradip Rath, Head of Department, Chemical Engineering, for letting me use all the required facilities in the department whenever I needed them. Also, Prof. Sandip Khan has been an immense help whenever I needed his help for running my simulations in the Undergraduate Computer Laboratory. He let us use the lab computers even in the weekends when we needed it the most. I would also like to take this opportunity to thank all the staff of the Chemical Engineering Department for ensuring that all the equipment in lab were in proper working order.

Last, I would like to express my gratitude towards my colleagues Mr. Ashis Kumar and Ms. Swetashree Sahoo for helping me in the project work whenever I needed any. I am also grateful to my parents for providing the moral support, whenever I needed it the most.

May 11, 2016 *Sidhartha Tirthankar*

NIT Rourkela Roll Number: 112CH0101

Abstract

Extensive research has been done on external flow of fluids over variously shaped bodies as is evident from the extensive literature available for circular cylinder and spheres, for instance. However, much of the literature has focused only on Newtonian fluid flow, leaving non-Newtonian fluid behavior out of the picture. In daily life we encounter non-Newtonian fluids like slurries, foams, emulsions etc. Also, much of the research has focused on circular cylinders, keeping elliptical cylinder data scant. Hence, the objective of this project is to emphasize on the flow pattern of Non-Newtonian fluids across elliptical cylinders and encourage further advancement in the same.

Steady-state unconfined flow over a two-dimensional elliptical cylinder (E=0.5, 2) has been investigated by using ANSYS Fluent (version 15.0) in the laminar flow regime. The influence of aspect ratio of the ellipse (E = 2, 0.5), Reynolds number ($5 \leq Re \leq 40$) and power-law index (0.8, 1, 1.2) on the flow phenomena like drag coefficient and pressure drag coefficient has been studied. It was found that the influence of Reynolds number and power-law index was somewhat of a complex nature on the drag and pressure drag coefficients.

Steady-state unconfined flow over rotating circular cylinder has been investigated by using the Multiple Reference Frame (MRF) model using ANSYS Fluent (version 15.0) in the two dimensional laminar flow regime for Re = 10 and 40 and dimensionless rotational speed α = 2, 4 and 6. The optimum size of rotating domain found for the rotating circular cylinder problem was used to simulate an unconfined flow around rotating elliptical cylinder in the two dimensional laminar flow regime for $10 \leq Re \leq 40$ and $2 \leq \alpha \leq 6$.

All the data obtained for the static elliptical cylinder has been matched with their corresponding values in the literature. Data obtained for unconfined rotating elliptical cylinder by using MRF model has not been reported in literature yet. The new data obtained can be used for the transient simulation of the same problem by using a sliding mesh approach.

Keywords: Power-law fluids; Elliptical cylinders; Drag coefficients; Pressure drag coefficients; Lift coefficients; Rotating cylinders; Multiple Reference Frame.

Contents

List of Figures

List of Tables

Nomenclature

a	=	length of semi-minor axis of ellipse (m)
b	=	length of semi-major axis of ellipse (m)
C_D	=	Drag coefficient
C_{DP}	=	Pressure drag coefficient
C_{DF}	=	Wall drag coefficient
C_L	=	Lift coefficient
D, D'	=	Diameter of circle (m)
E	=	Aspect ratio of ellipse
f	=	Body force
F_D	=	Drag force per unit length of cylinder (N/m)
F_{DP}	=	Pressure component of drag force per unit length of cylinder (N/m)
F_L	=	Lift force per unit length of cylinder (N/m)
m	=	Power-law consistency index (Pa s^n)
n	=	Power-law index
P, p	=	Pressure (Pa)
R	=	Radius of circle (m)
Re	=	Reynolds number
u	=	Velocity (m/s)
U_x	=	x-velocity (m/s)
U_y	=	y-velocity (m/s)
U_∞, U_0	=	Uniform velocity of fluid at inlet (m/s)

Greek letters

α	=	Dimensionless rotational velocity
ε	=	Rate of strain tensor
ρ	=	Density (kg/m^3)
θ	=	Angle of inclination with –ve x-axis
σ	=	Stress tensor
τ	=	Shear stress
μ, η	=	Dynamic viscosity (Pa s)
Ω	=	Angular velocity of cylinder (rad/s)

Chapter 1

Introduction

Study of external fluid flow over various shaped bodies has a special importance within the domain of fluid mechanics and transport phenomena. The flow over a circular cylinder has provided a fundamental understanding of the various phenomena that take place during fluid flow over bluff bodies like, nature of flow close to the solid surface, flow separation, wake dynamics (size, volume, shape, etc.), vortex shedding characteristics, and laminar-turbulent transitions, etc.

The environment contains a variety of fluids, both Newtonian and Non-Newtonian. We find numerous situations where fluid dynamics need to be applied and studied. However, there is an inherent problem while studying fluid flows; not only are these invisible to the naked eye, but also it is of immense difficulty to understand the following characteristics pertaining to fluid flows:

(i) They are highly deformable as compared to their solid counterparts and this deformity of theirs depend on a physical property also known as viscosity.
(ii) Fluid flows next to a solid is a very common example that can be found in the nature. This includes complex phenomena like the no-slip condition in which the layer of a fluid just adjacent to the solid surface sticks to it and has zero relative velocity, the formation of boundary layers and their separation.
(iii) The fuzzy zone in which laminar flow and turbulent flow are hard to distinguish is still under the radar of scientists.

Due to these enumerated phenomena, applying fluid dynamics to practical situations is not so easy. [1] Macroscopic fluid dynamics study cannot be used to predict flow patterns of fluids over various shaped bodies since that branch of science focuses on bulk momentum transport. Computational Fluid Dynamics, however, is the perfect tool to predict flow patterns of both Newtonian and Non-Newtonian fluid flows by discretizing the spatial domain into a grid and computing the governing equations for individual cells. Thus, instead of solving the continuous governing partial differential equations, we create approximate, discretized versions, and solve those. Some popular CFD software are FLUENT, OpenFOAM, OpenFlower, FLOW3D etc.

1.1 Flow Regimes

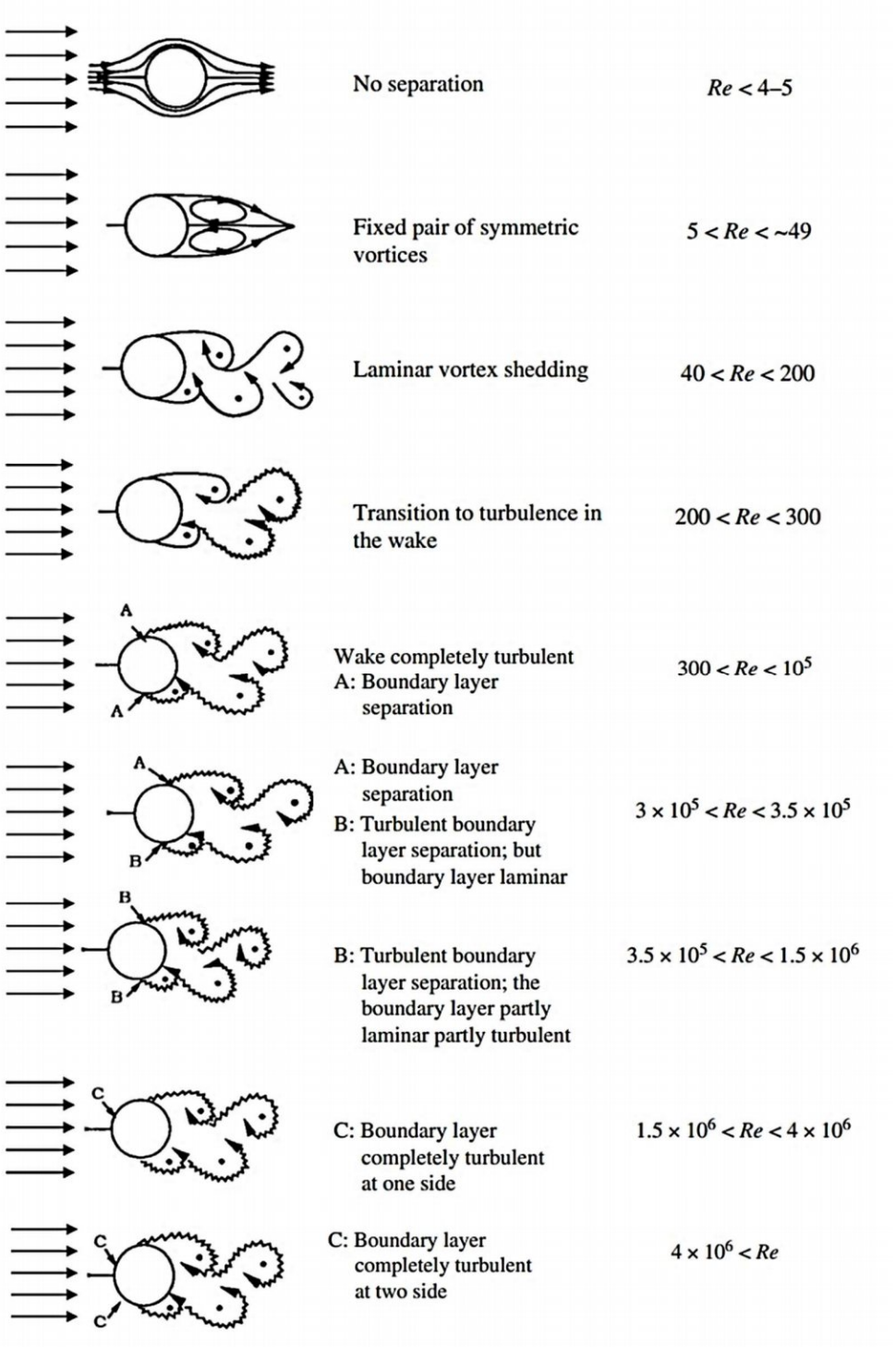

Figure 1.1: Schematics of the different flow regimes past an unconfined circular cylinder. Source: Adapted from Ref. [2]

For a fully developed Laminar flow, the streamlines stay attached to the shape of the object and separation does not take place.

As the Reynolds number increases beyond 1, the flow pattern behind the cylinder becomes different from that in front of it. At a Reynolds number of about 10, a zone of recirculating flow develops near the rear portion.

The recirculation zone (also known as wake) increases in size with increasing Reynolds number, and at Re=100, it covers nearly one-half of the cylinder. The large eddies or vortices in the wake constantly dissipate mechanical energy and cause the pressure at that location to be much less than the upstream pressure. This makes the form drag (due to pressure) quite large relative to the drag caused by wall shear (viscosity).

At moderate Reynolds number of 200 to 300, oscillations develop in the wake and vortices get dismantled from the wake in a periodic fashion, forming in the downstream fluid a series of moving vortices or a "vortex street", also known as the von Kármán vortex street.

For $Re=10^4$, the boundary layer on the front part of the cylinder is still laminar and the angle of separation becomes approximately 85º.

For $Re=10^6$ and higher, the separation point moves toward the rear end of the cylinder and the wake size shrinks. [3]

Currently only scant results are available for flow across elliptical, square, equilateral triangular and semi-circular cylinders. Most of these investigations are limited only to the onset of flow separation and the laminar vortex shedding regimes. In Non-Newtonian fluids the literature is even more scanty. Even more scant results are available for flow around rotating or translating cylinders. Our objective here is to find out the flow phenomena of a rotating elliptical cylinder by using the multiple reference frame (MRF) model. Being an approximation, this model is expected to give results that are in the range of 5% error, but since the alternate, the sliding mesh method is computationally time consuming, a MRF model can be used to build an idea of the results that can be expected from a more robust sliding mesh model.

1.2 Governing Equations

Let us consider the flow of incompressible fluids past a cylinder of circular shape which is infinitely long in neutral direction.

We take some simplifying assumptions:

(i) The fluid is incompressible.
(ii) Viscosity does not vary with time or temperature.

Within this framework of simplifying assumptions, the momentum characteristics of fluid flow over a two-dimensional immersed cylinder of an arbitrary cross section are written as follows:

Continuity equation:

$$\boldsymbol{\nabla}.\boldsymbol{u} = 0 \tag{1.1}$$

Momentum equation:

$$\rho(\boldsymbol{u}.\boldsymbol{\nabla}\boldsymbol{u} - \boldsymbol{f}) - \boldsymbol{\nabla}.\boldsymbol{\sigma} = 0 \tag{1.2}$$

where σ is the stress tensor, ρ is the density of the fluid, f is the body force, and u is the velocity of the fluid.

1.3 Elliptical Cylinders

An elliptical cylinder indicates the simplest departure from a circular one. It retains some geometrical features of the circular cylinder, for example, it is also free of sharp corners and edges like its circular counterpart. An elliptical cylinder can be defined with the help of two geometric parameters (minor and major axis, or aspect ratio, E). $E=1$ denotes a circular shape and $E \rightarrow 0$ or $E \rightarrow \infty$ denote a plate oriented along and transverse to the direction of flow. Slender configuration ($E>1$) aligned with the flow will behave more like a streamlined object, whereas the blunt configuration ($E<1$) will behave like a bluff body.

1.4 The Power-law Model

The power-law model, also known as the Ostwald-de Waele model, is a type of generalized model which covers both Newtonian and non-Newtonian fluids. According to this model, the shear stress, τ, is given by

$$\boldsymbol{\tau} = 2\eta\boldsymbol{\varepsilon}(\boldsymbol{u}) \tag{1.3}$$

where ε(u), the components of the rate of strain tensor, is given by

$$\boldsymbol{\varepsilon}(\boldsymbol{u}) = \frac{1}{2}\{(\boldsymbol{\nabla u}) + (\boldsymbol{\nabla u})^T\} \tag{1.4}$$

The viscosity, η, is given by

$$\eta = m\left(\frac{I_2}{2}\right)^{\frac{n-1}{2}} \tag{1.5}$$

where m is the power-law consistency index and n is the power-law index of the fluid; and I_2 is the second invariant of the rate of strain tensor (ε), given by

$$I_2 = \left(\boldsymbol{\varepsilon}_{xx}^2 + \boldsymbol{\varepsilon}_{yy}^2\right) + \left(\boldsymbol{\varepsilon}_{xy}^2 + \boldsymbol{\varepsilon}_{yx}^2\right) \tag{1.6}$$

and the velocity components can be linked to the rate of strain components by the following equations

$$\boldsymbol{\varepsilon}_{xx} = \frac{\partial \boldsymbol{U_x}}{\partial x}, \quad \boldsymbol{\varepsilon}_{yy} = \frac{\partial \boldsymbol{U_y}}{\partial y}, \quad \boldsymbol{\varepsilon}_{xy} = \boldsymbol{\varepsilon}_{yx} = \frac{1}{2}\left(\frac{\partial \boldsymbol{U_x}}{\partial y} + \frac{\partial \boldsymbol{U_y}}{\partial x}\right) \tag{1.7}$$

The power-law model is useful because of its simplicity. It describes the flow of real non-Newtonian fluid only approximately, because it predicts that fluids can have infinite or zero viscosity at some specified conditions. This, however, is practically impossible owing to physical chemistry of the fluid at a molecular level.

Power-law fluids can be divided into three types depending on the value of power-law or flow behavior index, n.

(i) Pseudoplastic or shear thinning (n < 1)
Examples: ketchup, whipped cream, blood

(ii) Newtonian (n = 1)
Examples: water, blood plasma

(iii) Dilatant or shear thickening (n > 1)
Examples: suspensions of corn starch in water, wet sand on a beach

1.5 Overview of Moving Zone Approaches

The Fluent software module consists of a powerful set of features to address the motion of both translating and rotating moving cell zones.

Two kinds of moving flows can be accessed using this feature:

(i) Rotating or translating flow in a single reference frame
(ii) Rotating or translating flow in multiple reference frames

Aforementioned first type of problem can be used to model flows in turbo machinery, mixing tanks and related devices. In all the stated cases, the flow is unsteady in an inertial frame, because the rotor/impeller blades sweep the domain periodically. However, in the absence of strong interactions with stators, it is possible to perform calculations in a domain that moves with the rotating portion, so the flow behaves like a steady-state flow relative to the non-inertial rotating frame, hence the analysis of flow gets simplified to a great extent.

If in addition to the rotating flow, strong interactions are present in the form of static components like stators, then the problem becomes impossible to solve by assuming a single rotating frame of reference that rotates with the rotor. This phenomenon is observed when the rotating and static parts are close to one another leading to strong interaction forces. Three approaches are provided by Fluent to solve the aforementioned types of flow:

(i) the multiple reference frame (MRF) model
(ii) the mixing plane model
(iii) the sliding mesh model

Both the multiple reference frame and mixing plane model are steady-state approximation models. These two models take approximate means to account for weak interactions caused by rotating and static parts in a fluid flow. Most engineering problems are solved by using these methods due to their inherent simplicity for example simulating a HVAC system to find stagnant zones in a building. On the other hand, the sliding mesh model is a transient model which considers all the static and rotating part interactions in the fluid flow. It is more computationally demanding than the other two models and gives a fairly accurate picture of the real transient flow.

Chapter 2

Literature Review

Some early studies by Imai [4] and Hasimoto [5], have used Oseen's linearization analysis to obtain the expressions for hydrodynamic drag applicable at low Reynolds number for elliptical cylinders. Some of the initial studies on numerical solutions of the governing differential equations for elliptical cylinders are due to Lugt and Haussling [6], and Meller [7]. Many others, see Refs. [8-15], have reported numerical solutions at relatively low Reynolds numbers ranging from $1 \leq Re \leq 200$.

The following studies have been done for Newtonian fluid flow around an unconfined elliptical cylinder. Johnson et al. [8] have presented studies on vortex structures behind 2D elliptical cylinders at low Reynolds numbers (Re=30-200). They found out that the value of Reynolds number at the onset of periodic vortex shedding decreased by decreasing the aspect ratio (E) of the ellipse. Faruquee et al. [10] have presented studies on flow around an elliptical cylinder in the laminar region and its changes pertaining to changes in aspect ratio of the ellipse. They varied the aspect ratio from 0.3 to 1 for a Reynolds number of 40. They found out that a pair of steady vortices formed only when they increased the aspect ratio to 0.34; below that value, no vortices were found behind the elliptical cylinder. Stack and Bravo [11] have presented studies on the flow separation behind elliptical cylinders at Reynolds number less than 10 (Re=1-10). They found out that at Reynolds number greater than one, the relationship between critical aspect ratio and Reynolds number was linear. Patel [13] has presented studies on the flow around an elliptic cylinder which has been impulsively started at various angles of attack (ranging from 0° to 90° incidence). He found out that a vortex street developed for Reynolds number 60 and 200 at 45 and 30° incidence. D'Alessio and Dennis [14] developed a vorticity model for viscous flow past a cylinder and reported good values for an inclined elliptical cylinder. Dennis and Young [15] have presented studies on steady-state fluid flow past an elliptical cylinder which has been inclined (ranging from 0° to 90°) to the stream for Reynolds number up to 40. They found asymmetric flows for all inclinations except at 90°, which has symmetric vortices behind the elliptical cylinder.

Meanwhile, only three studies have been done on unconfined power-law fluid flow around an elliptical cylinder [12, 16, 17].

Rao et al. [12] have carried out extensive numerical simulations of 2-D laminar flow of power-law fluids over elliptical cylinders with different aspect ratios to establish the conditions for onset of wake formation and vortex shedding. They have reported influence of the aspect ratio ($0.2 \leq E \leq 5$) and power-law index ($0.3 \leq n \leq 1.8$) on the critical values of the Re, denoting vortex shedding and the onset of flow separation. Plots denoting the vorticity profiles and flow separation showing vortex shedding phenomena have been reported by them. They found out that the onset of wake formation and vortex shedding are both postponed to higher Reynolds number for shear-thinning fluids as compared to those in shear-thickening fluids.

Sivakumar et al. [16] have numerically investigated power-law fluid flow past an unconfined elliptic cylinder in the 2-D steady-state cross-flow regime. The influence of the aspect ratio of ellipse ($0.2 \leq E \leq 5$), power-law index ($0.2 \leq n \leq 1.8$) and Reynolds number ($0.01 \leq Re \leq 40$) on the flow characteristics has been reported by them. Flow patterns showing vorticity and streamline profiles, and the pressure distribution on the surface of the cylinder have also been reported by them. They found out that for aspect ratio $E > 1$ and shear-thinning behavior, the wake is shorter due to delay in flow separation; and, opposite behavior is obtained for $E < 1$ and shear-thickening behavior.

Forced convection heat transfer to power-law fluids from a heated elliptical cylinder in the steady-state, laminar cross-flow regime has been studied by Bharti et al. [17]. They have reported the effects of the aspect ratio of the elliptical cylinder ($0.2 \leq E \leq 5$), Reynolds number ($0.01 \leq Re \leq 40$), power-law index ($0.2 \leq n \leq 1.8$) and Prandtl number ($1 \leq Pr \leq 100$) on the average Nusselt number (Nu). According to them, heat transfer is enhanced by pseudoplastic fluids, while it is reduced in dilatant fluids.

A study on flow past an elliptical cylinder undergoing rotationally oscillatory motion has been done by Alawadhi [20]. He has used the finite element method to simulate the near-wake of an elliptical cylinder undergoing rotationally oscillating motion at low Reynolds number, $50 \leq Re \leq 150$. According to his studies, increasing the Reynolds number increased the RMS of lift coefficient and decreased the average of drag coefficient.

The objective of this study is to first establish the relationship between power-law index and Reynolds number on drag and pressure drag coefficients for the flow past a static elliptical cylinder. Further, studies on a rotating elliptical cylinder will also been carried out by using the MRF steady-state approximation method. The optimum domain size for MRF being found out by comparing data for a rotating circular cylinder which has already been carried out by Panda and Chhabra [19].

Chapter 3

Mathematical Formulation

3.1 Lid-driven Flow in a Square Cavity

The lid-driven square cavity flow problem is a classical CFD problem. This works as a precursor to other complex simulations to verify that the author has sufficient acumen and experience to work on complex CFD problems.

A square cavity (Fig. 3.1) is filled with an incompressible fluid. The top wall of the square cavity moves with a constant velocity. For Re = 100, 400 and 1000, streamlines in the square cavity, x-velocity along vertical line through geometric centre of cavity and y-velocity along horizontal line through geometric centre of cavity have been plotted.

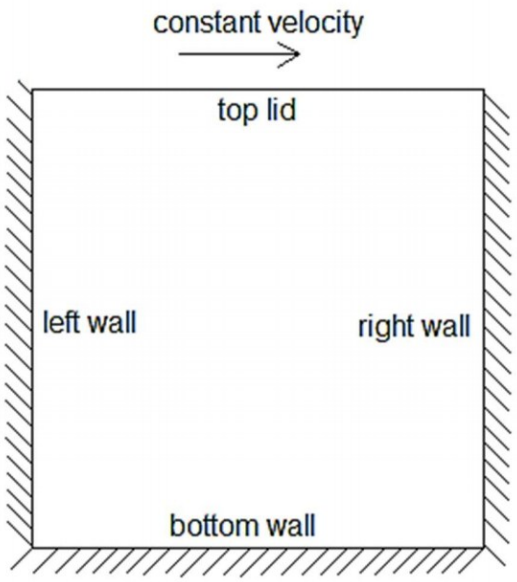

Figure 3.1: Schematic representation of lid-driven square cavity flow

3.1.1 Boundary Conditions

(1) Top lid: no-slip, constant velocity in x-direction depending on Re

$$U_x = U_0 \quad and \quad U_y = 0$$

(2) Left wall: no-slip, stationary wall

$$U_x = 0 \quad and \quad U_y = 0$$

(3) Bottom wall: no-slip, stationary wall

$$U_x = 0 \quad and \quad U_y = 0$$

(4) Right wall: no-slip, stationary wall

$$U_x = 0 \quad and \quad U_y = 0$$

3.1.2 Numerical Methodology

The current numerical simulation has been carried out by using ANSYS Fluent (v. 15.0). For evaluating the results, a uniform mesh having 129x129 points was used for the computational domain as suggested by Ghia et al. [18]. The 2-D, steady-state, laminar segregated solver was used with second order upwind scheme for taking care of the convective terms. For pressure-velocity coupling, the semi-implicit method for the pressure linked equations (SIMPLE) scheme was used. For the x-component and y-component of velocity and continuity, a convergence criterion of 10^{-5} was used.

3.1.3 Choice of Numerical Parameters

Since results will be obtained as a function of dimensionless Reynolds number, so all numerical parameters were chosen so as to get Re = 100, 400 and 1000.

Since a uniform mesh of 129x129 points was used, so each quadrilateral is a square with its side as (1/128)th times the side of the square domain.

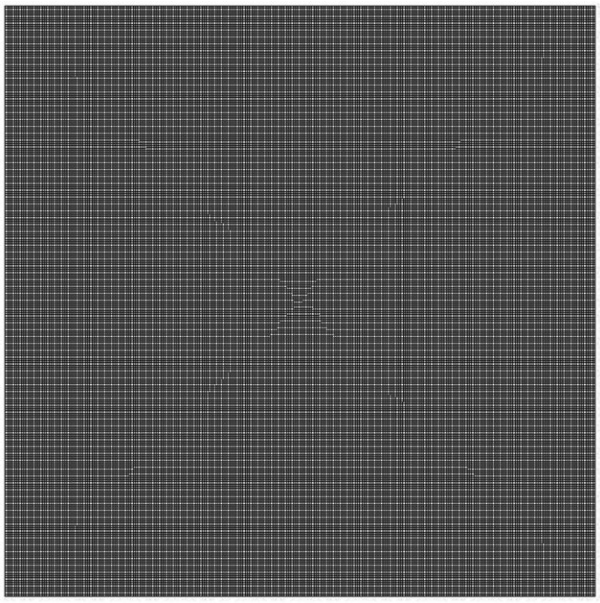

Figure 3.2: Grid representation of lid-driven square cavity

3.2 Flow around an Elliptical Cylinder

For a power-law n = 0.8, 1, 1.2 fluid flow across an elliptical cylinder having aspect ratio E = 0.5, 2, streamlines were found out for Re = 5, 10, 20, 30, 40. Also, the values of drag coefficient (C_D) and pressure drag coefficient (C_{DP}) were found out and plotted to see the variation from literature values.

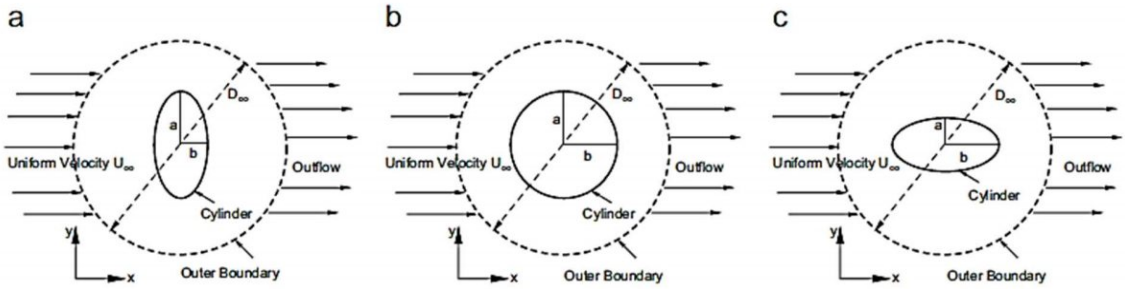

Figure 3.3: Schematic representation of flow around an elliptical cylinder for (a) E < 1, (b) E = 1, and (c) E > 1; adapted from Ref. [16]

For power-law fluids the Reynolds number (Re) is defined as:

$$Re = \frac{\rho(2a)^n U_\infty^{2-n}}{m} \tag{3.1}$$

Total drag coefficient (C_D) is defined as:

$$C_D = \frac{2F_D}{\rho U_\infty^2 a} = C_{DP} + C_{DF} \tag{3.2}$$

where F_D is the drag force acting per unit length of the cylinder, C_{DP} is the pressure drag coefficient and C_{DF} is the friction drag coefficient.

Pressure drag coefficient (C_{DP}) is defined as:

$$C_{DP} = \frac{2F_{DP}}{\rho U_\infty^2 a} \tag{3.3}$$

Where F_{DP} is the pressure portion of the drag force acting per unit length of the cylinder.

3.2.1 Boundary Conditions

Using a circular mesh rather than a rectangular one has certain advantages. A circular mesh has one semi-circular arc as the inlet and the other as the outlet. There are no specified shear (slip) walls like in a rectangular mesh. The sizing of a circular mesh also becomes simpler owing to the fact that it has only one parameter (diameter) that can be varied.

(1) Inlet plane: Uniform velocity in x-direction

$$U_x = U_\infty \quad and \quad U_y = 0$$

(2) Surface of the elliptical cylinder: The no slip boundary condition is used

$$U_x = 0 \quad and \quad U_y = 0$$

(3) Outlet plane: The outflow boundary condition is used. Indicating that the outflow conditions have very little effect on the upstream flow since the conditions at the outflow are extrapolated.

$$\frac{\partial U_x}{\partial x} = 0 \quad and \quad \frac{\partial U_y}{\partial x} = 0$$

3.2.2 Numerical Methodology

The current numerical simulation has been carried out by using ANSYS Fluent (v. 15.0). For evaluating the results, unstructured quadrilateral cells were generated by the help of Meshing software of ANSYS Workbench, which was used for the computational domain. The mesh near the surface of the cylinder was kept sufficiently refined for resolving the boundary layer. The 2-D, steady-state, laminar segregated solver was used with second order upwind scheme for taking care of the convective terms. For pressure-velocity coupling, the semi-implicit method for the pressure linked equations (SIMPLE) scheme was used. For the x-component and y-component of velocity and continuity, a convergence criterion of 10^{-10} was used.

3.2.3 Choice of Numerical Parameters

The reliability and accuracy of the results is dependent on an optimal choice of domain and grid size. A very large value of D_∞ will require enormous computational resources and a small value will unduly influence the results. $D_\infty/(2a) = 300$ as suggested by Sivakumar et al. [16] was used for the current simulation. On the cylinder wall, 200 elements were specified with a growth rate of 1.02. A refinement of 3 was also used on the cylinder wall to ensure fineness of grid near the wall.

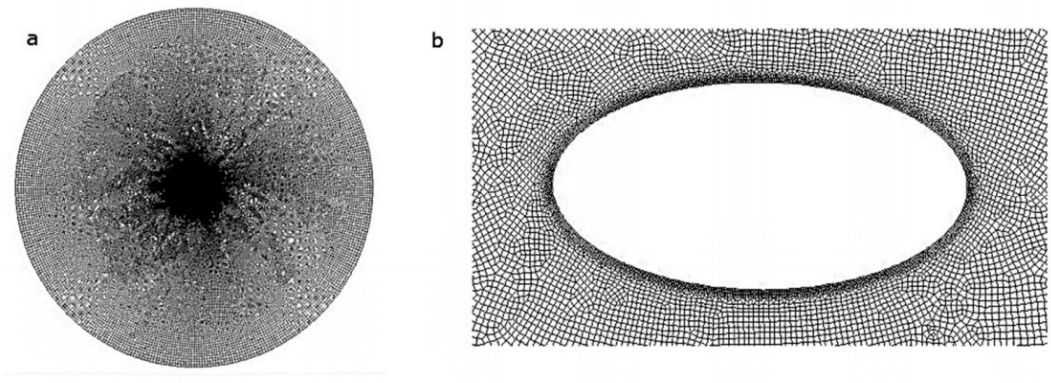

Figure 3.4: Grid representation of (a) entire mesh, (b) mesh near cylinder wall for elliptical cylinder

3.3 Flow around a Rotating Circular Cylinder

For a Newtonian fluid flow across a rotating circular cylinder, streamlines were found out for Re = 10, 40; α = 2, 4, 6. Also, the drag coefficient (C_D) and lift coefficient (C_L) were found out and variation from literature values were measured as error. Then, a MRF model was tried with the same rotating circular cylinder by varying the diameter of the rotating domain D' = 1.2xD, 1.1xD, 1.05xD, 1.02xD, 1.01xD. Drag coefficient (C_D) and lift coefficient (C_L) were found out and error of 5% was set as an acceptable value since MRF is an approximate model. The best rotating domain was found out which could be used to simulate an MRF model of a rotating elliptical cylinder.

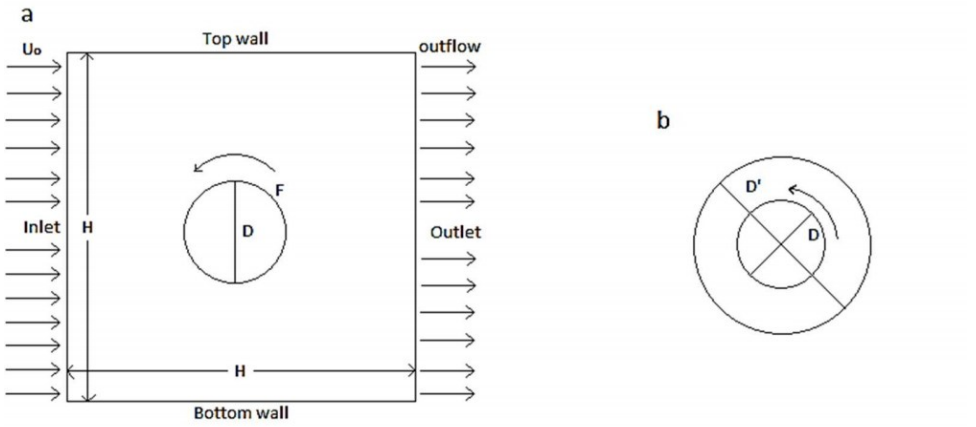

Figure 3.5: Schematic representation of (a) rotating circular cylinder, (b) MRF model close-up

The Reynolds number (Re) for the given problem is defined as:

$$Re = \frac{\rho U_o D}{\mu} \tag{3.4}$$

The dimensionless rotational speed (α) is defined as:

$$\alpha = \frac{R\Omega}{U_o} \tag{3.5}$$

Total drag coefficient (C_D) is defined as:

$$C_D = \frac{2F_D}{\rho U_o^2 D} \tag{3.6}$$

where F_D is the drag force acting per unit length of the cylinder in the direction of flow.

Total lift coefficient (C_L) is defined as:

$$C_L = \frac{2F_L}{\rho U_o^2 D} \tag{3.7}$$

where F_L is the lift force acting per unit length of the cylinder in the y-direction.

3.3.1 Boundary Conditions

(1) Inlet plane: Uniform velocity in x-direction

$$U_x = U_0 \quad and \quad U_y = 0$$

(2) Surface of the rotating circular cylinder: The no slip boundary condition is used

$$U_x = U_0\, \alpha \sin\theta \quad and \quad U_y = U_0\, \alpha \cos\theta$$

(3) Top and bottom wall: These are assumed to be slip boundaries

$$\frac{\partial U_x}{\partial y} = 0 \quad and \quad U_y = 0$$

(4) Outlet plane: The outflow boundary condition is used. Indicating that the outflow conditions have very little effect on the upstream flow since the conditions at the outflow are extrapolated.

$$\frac{\partial U_x}{\partial x} = 0 \quad and \quad \frac{\partial U_y}{\partial x} = 0$$

3.3.2 Numerical Methodology

The current numerical simulation has been carried out by using ANSYS Fluent (v. 15.0). For evaluating the results, unstructured quadrilateral cells were generated by the help of Meshing software of ANSYS Workbench, which was used for the computational domain. The mesh near the surface of the cylinder was kept sufficiently refined for resolving the boundary layer. The 2-D, steady-state, laminar segregated solver was used with second order upwind scheme for taking care of the convective terms. For pressure-velocity coupling, the semi-implicit method for the pressure linked equations (SIMPLE) scheme was used. For the x-component and y-component of velocity and continuity, a convergence criterion of 10^{-8} was used.

3.3.3 Choice of Numerical Parameters

The accuracy and reliability of the numerical results is dependent on an optimal choice of domain and grid size. A square domain with a very large value of H will require enormous computational resources and a small value will unduly influence the results. H/D = 100 as suggested by Panda and Chhabra [19] was used for the current simulation. On the cylinder wall, 200 elements were specified with a growth rate of 1.01. A refinement of 3 was also used on the cylinder wall to ensure fineness of grid near the wall. For the MRF model, a concentric circular domain was chosen which rotated at the same constant rotational speed. The diameter of the rotating domain was changed to determine the optimum size to produce best results (error < 5%).

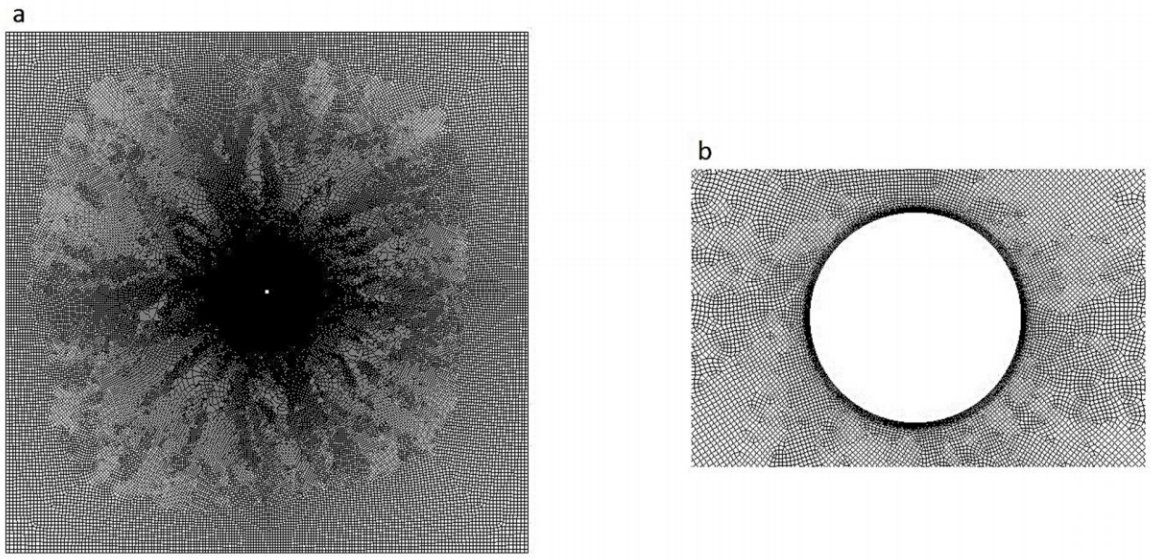

Figure 3.6: Grid representation of (a) entire mesh, (b) mesh near cylinder wall for rotating circular cylinder

3.4 Flow around a Rotating Elliptical Cylinder

The MRF model was used for simulating the rotating elliptical cylinder. The rotating domain's (circular) diameter was set to D = 1.01*(2b), which was found out from the results of the rotating circular cylinder. For the flow of a Newtonian fluid, C_D and C_L values were found out for Re = 10, 20, 30, 40; α = 2, 4, 6; θ = 0º, 30º, 60º, 90º, 120º, 150º. Streamlines for the extreme conditions of flow were also found.

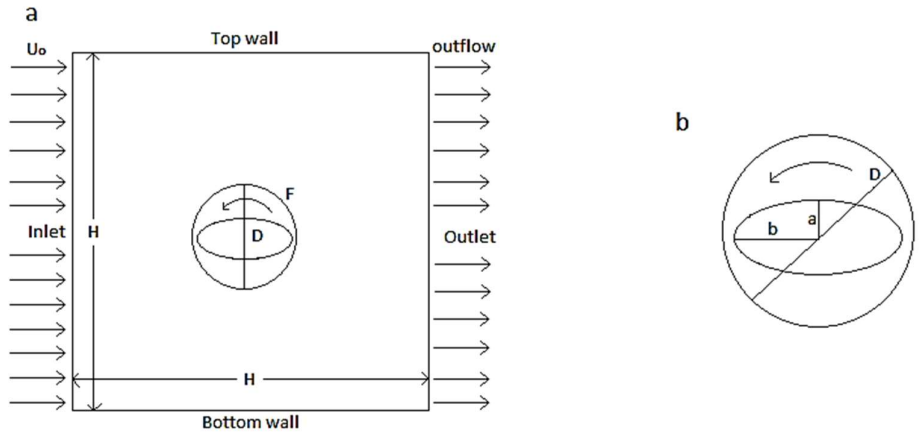

Figure 3.7: Schematic representation of (a) rotating elliptical cylinder, (b) MRF model close-up

The Reynolds number (Re) for the given problem is defined as:

$$Re = \frac{\rho U_o D}{\mu} \tag{3.8}$$

The dimensionless rotational speed (α) is defined as:

$$\alpha = \frac{R\Omega}{U_o} \tag{3.9}$$

Total drag coefficient (C_D) is defined as:

$$C_D = \frac{2F_D}{\rho U_o^2 D} \tag{3.10}$$

where F_D is the drag force acting per unit length of the cylinder in the direction of flow.

Total lift coefficient (C_L) is defined as:

$$C_L = \frac{2F_L}{\rho U_o^2 D} \tag{3.11}$$

where F_L is the lift force acting per unit length of the cylinder in the y-direction.

3.4.1 Boundary Conditions

(1) Inlet plane: Uniform velocity in x-direction

$$U_x = U_0 \quad and \quad U_y = 0$$

(2) Surface of the rotating elliptical cylinder: The no slip boundary condition is used with a zero rotational velocity relative to the adjacent rotating cell zone.

(3) Top and bottom wall: These are assumed to be slip boundaries

$$\frac{\partial U_x}{\partial y} = 0 \quad and \quad U_y = 0$$

(5) Outlet plane: The outflow boundary condition is used. Indicating that the outflow conditions have very little effect on the upstream flow since the conditions at the outflow are extrapolated.

$$\frac{\partial U_x}{\partial x} = 0 \quad and \quad \frac{\partial U_y}{\partial x} = 0$$

3.4.2 Numerical Methodology

The current numerical simulation has been carried out by using ANSYS Fluent (v. 15.0). For evaluating the results, unstructured quadrilateral cells were generated by the help of Meshing software of ANSYS Workbench, which was used for the computational domain. The mesh near the surface of the cylinder was kept sufficiently refined for resolving the boundary layer. The 2-D, steady-state, laminar segregated solver was used with second order upwind scheme for taking care of the convective terms. For pressure-velocity coupling, the semi-implicit method for the pressure linked equations (SIMPLE) scheme was used. For the x-component and y-component of velocity and continuity, a convergence criterion of 10^{-8} was used.

3.4.3 Choice of Numerical Parameters

The accuracy and reliability of the numerical results is dependent on an optimal choice of domain and grid size. A square domain with a very large value of H will require enormous computational resources and a small value will unduly influence the results. H/D = 100 was used for the current simulation. On the cylinder wall, 500 elements were specified with a growth rate of 1.02. A refinement of 3 was also used on the cylinder wall to ensure fineness of grid near the wall. For the MRF model, a concentric circular domain was chosen whose cell zone rotated at a constant rotational speed.

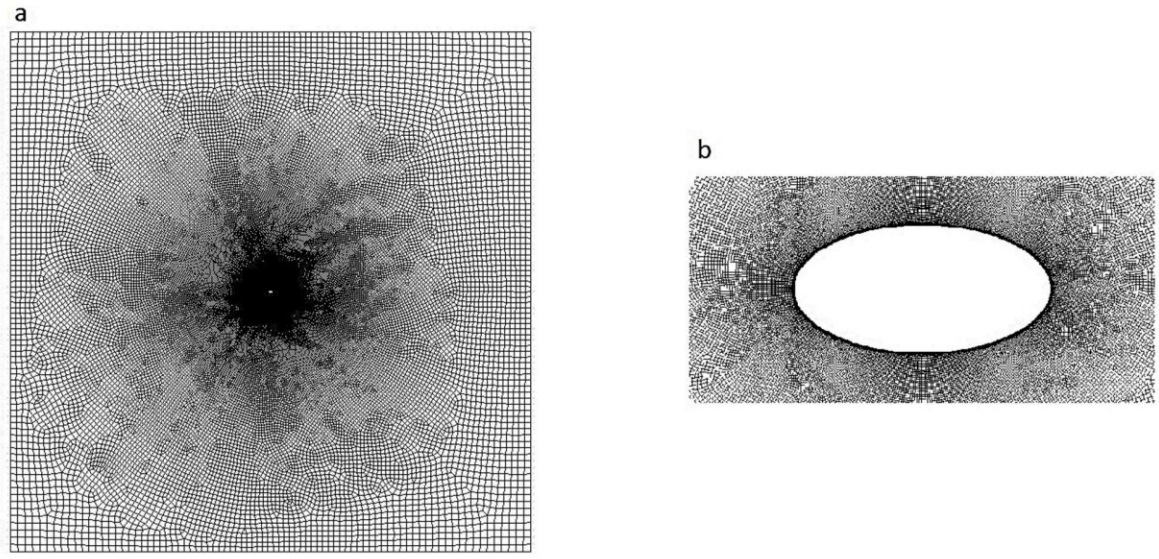

Figure 3.8: Grid representation of (a) entire mesh, (b) mesh near cylinder wall for rotating elliptical cylinder

Chapter 4

Results and Discussion

The following sections describe the results of various parameters obtained and their validation with the literature values. The dependence of flow phenomena like drag, pressure drag, and lift coefficient were found out and their dependence on fluid property like power-law index and flow characteristics like Reynolds number were found out.

4.1 Lid-driven Flow in a Square Cavity

Streamlines, x-velocity along vertical line and y-velocity along horizontal line through the geometric centre of the cavity were found out by varying the Reynolds number (Re = 100, 400 and 1000)

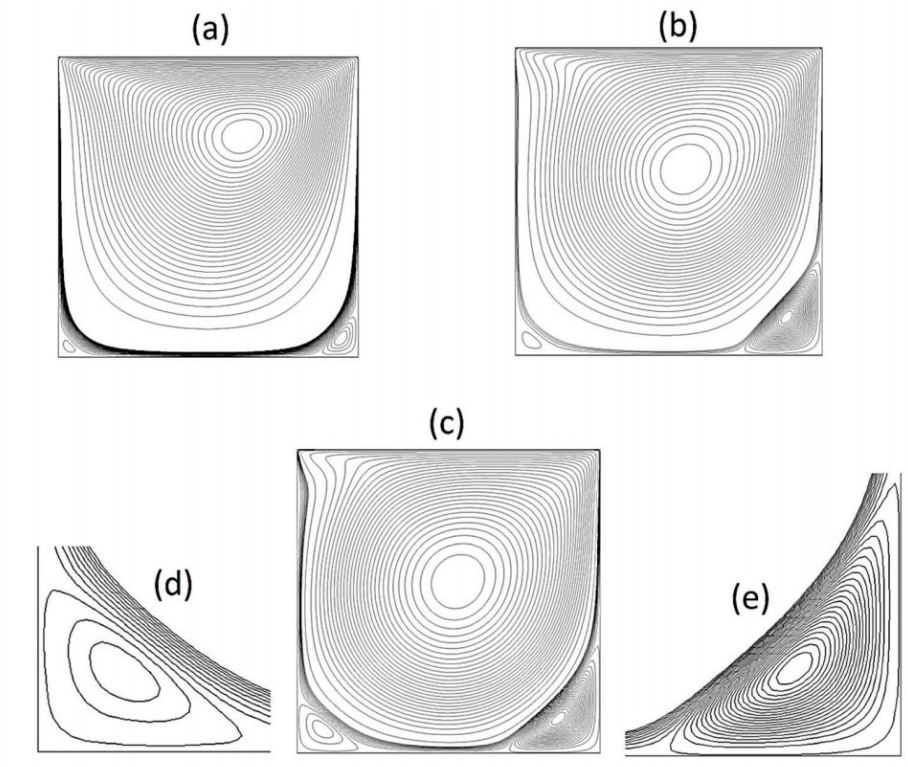

Figure 4.1: Streamlines for the lid-driven flow in a square cavity for (a) Re=100, (b) Re=400, (c) Re=1000; (d) bottom-left corner vortices for Re=1000, (e) bottom-right corner vortices for Re=1000

From the streamlines, it can be concluded that as Re increases, the size of the bottom-left and bottom-right corner vortices also increases. Also, by observing the streamlines of Re=1000, it can be postulated that at higher Re, a vortex region will also form in the top-left corner.

Table 4.1: Results for x-velocity along vertical line through geometric centre of cavity

129-grid point number	y	Re					
		100		400		1000	
		Present	Literature	Present	Literature	Present	Literature
129	1	1	1	1	1	1	1
126	0.9766	0.843118	0.84132	0.759856	0.75837	0.66251	0.65928
125	0.9688	0.791146	0.78871	0.686326	0.68439	0.579317	0.57492
124	0.9609	0.740157	0.73722	0.619873	0.61756	0.516574	0.51117
123	0.9531	0.69055	0.68717	0.561525	0.55892	0.472096	0.46604
110	0.8516	0.23519	0.23151	0.291767	0.29093	0.335967	0.33304
95	0.7344	0.0026131	0.00332	0.16222	0.16256	0.188063	0.18719
80	0.6172	-0.139762	-0.13641	0.0205149	0.02135	0.0564452	0.05702
65	0.5	-0.208166	-0.20581	-0.112993	-0.11477	-0.060318	-0.0608
59	0.4531	-0.21311	-0.2109	-0.172309	-0.17119	-0.108851	-0.10648
37	0.2813	-0.155976	-0.15662	-0.328076	-0.32726	-0.281033	-0.27805
23	0.1719	-0.100446	-0.1015	-0.24182	-0.24299	-0.386118	-0.38289
14	0.1016	-0.063562	-0.06434	-0.144277	-0.14612	-0.295113	-0.2973
10	0.0703	-0.046008	-0.04775	-0.101753	-0.15113	-0.217599	-0.2222
9	0.0625	-0.041418	-0.04192	-0.091147	-0.09266	-0.19716	-0.20196
8	0.0547	-0.03673	-0.03717	-0.080486	-0.08186	-0.176331	-0.18109
1	0	0	0	0	0	0	0

Table 4.2: Results for y-velocity along horizontal line through geometric centre of cavity

129-grid point number	x	Re					
		100		400		1000	
		Present	Literature	Present	Literature	Present	Literature
129	1	0	0	0	0	0	0
126	0.9688	-0.061841	-0.05906	-0.123915	-0.12146	-0.221974	-0.21388
125	0.9609	-0.077336	-0.07391	-0.159613	-0.15663	-0.285919	-0.27669
124	0.9531	-0.092661	-0.08864	-0.195985	-0.19254	-0.346989	-0.33714
123	0.9453	-0.107722	-0.10313	-0.232292	-0.22847	-0.401913	-0.39188
110	0.9063	-0.175889	-0.16914	-0.386962	-0.23827	-0.52138	-0.5155
95	0.8594	-0.232062	-0.22445	-0.451951	-0.44993	-0.426456	-0.42665
80	0.8047	-0.251756	-0.24533	-0.385325	-0.38598	-0.320045	-0.31966
65	0.5	0.0590818	0.05454	0.0533397	0.05188	0.0265272	0.02526
59	0.2344	0.177826	0.17527	0.302519	0.30174	0.324114	0.32235
37	0.2266	0.177599	0.17507	0.302854	0.30203	0.332666	0.33075
23	0.1563	0.163026	0.16077	0.282283	0.28124	0.374661	0.37095
14	0.0938	0.124949	0.12317	0.230415	0.22965	0.330626	0.32627
10	0.0781	0.110497	0.1089	0.209814	0.2092	0.307638	0.30353
9	0.0703	0.102407	0.10091	0.197669	0.19713	0.294003	0.29012
8	0.0625	0.0937135	0.09233	0.184052	0.1836	0.27845	0.27485
1	0	0	0	0	0	0	0

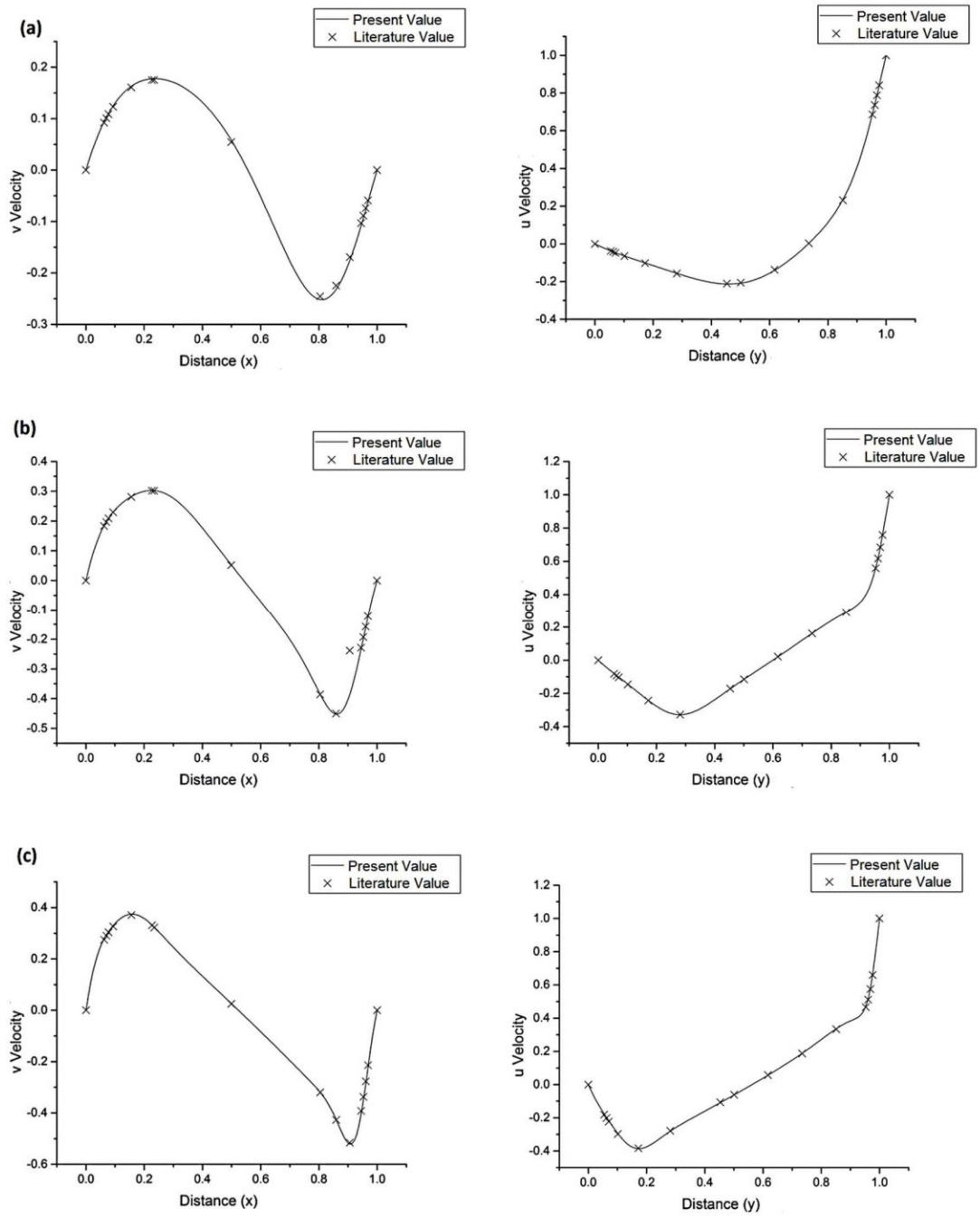

Figure 4.2: Velocity plots for the lid-driven flow in a square cavity at the geometrical centre lines (a) Re=100, (b) Re=400, (c) Re=1000

Almost all the calculated velocity values matched with the literature values with minimal errors. This indicates the adequacy of a 129x129 uniform mesh for finding out the solution of the given problem up to Re=1000.

From the velocity plots, we can conclude that the y-velocity along the horizontal line through geometric centre of cavity is almost symmetric as we travel from 0 to 1; the y-velocity at 0.8-0.9 region is higher than at the 0.2-0.3 region, due to the motion of the top lid from left to right direction. The same is, however, not true for the x-velocity along the vertical line through the geometric centre of cavity, since velocity values are higher near the moving top lid due to no-slip boundary condition at all the walls.

4.2 Flow around an Elliptical Cylinder

Flow phenomena like drag and pressure drag coefficients, and streamlines were found out for E = 2 (streamlined body) and E = 0.5 (bluff body) and their dependence on fluid property like power-law index and flow characteristic like Reynolds number were found out.

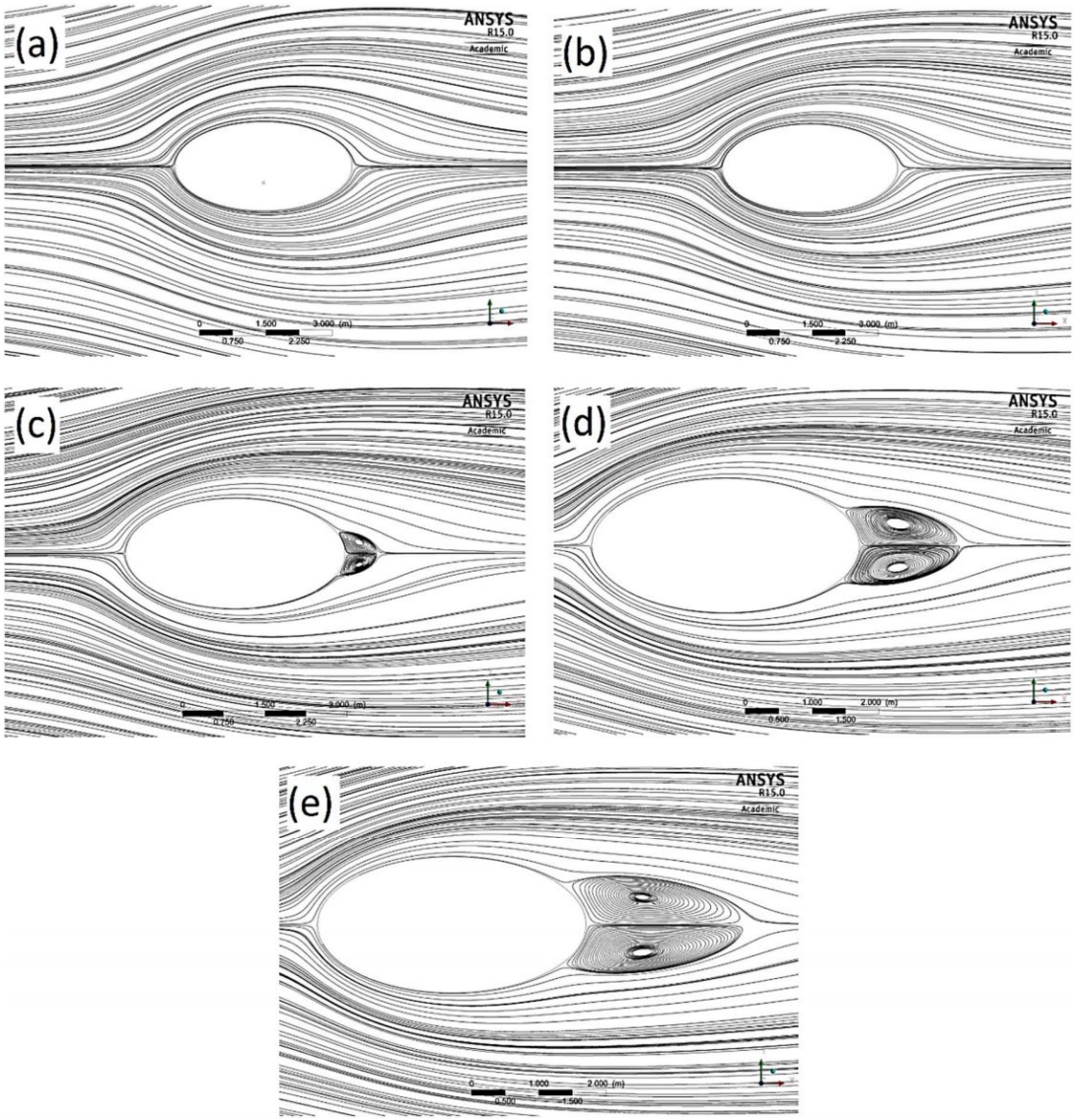

Figure 4.3: Streamlines for E=2, n=1 and (a) Re=5, (b) Re=10, (c) Re=20, (d) Re=30, (e) Re=40

The wake size increases with increase in Reynolds number. For E = 2 (i.e. E > 1) it is observed that the body acts like a streamlined object and smaller wakes are formed in comparison to E < 1.

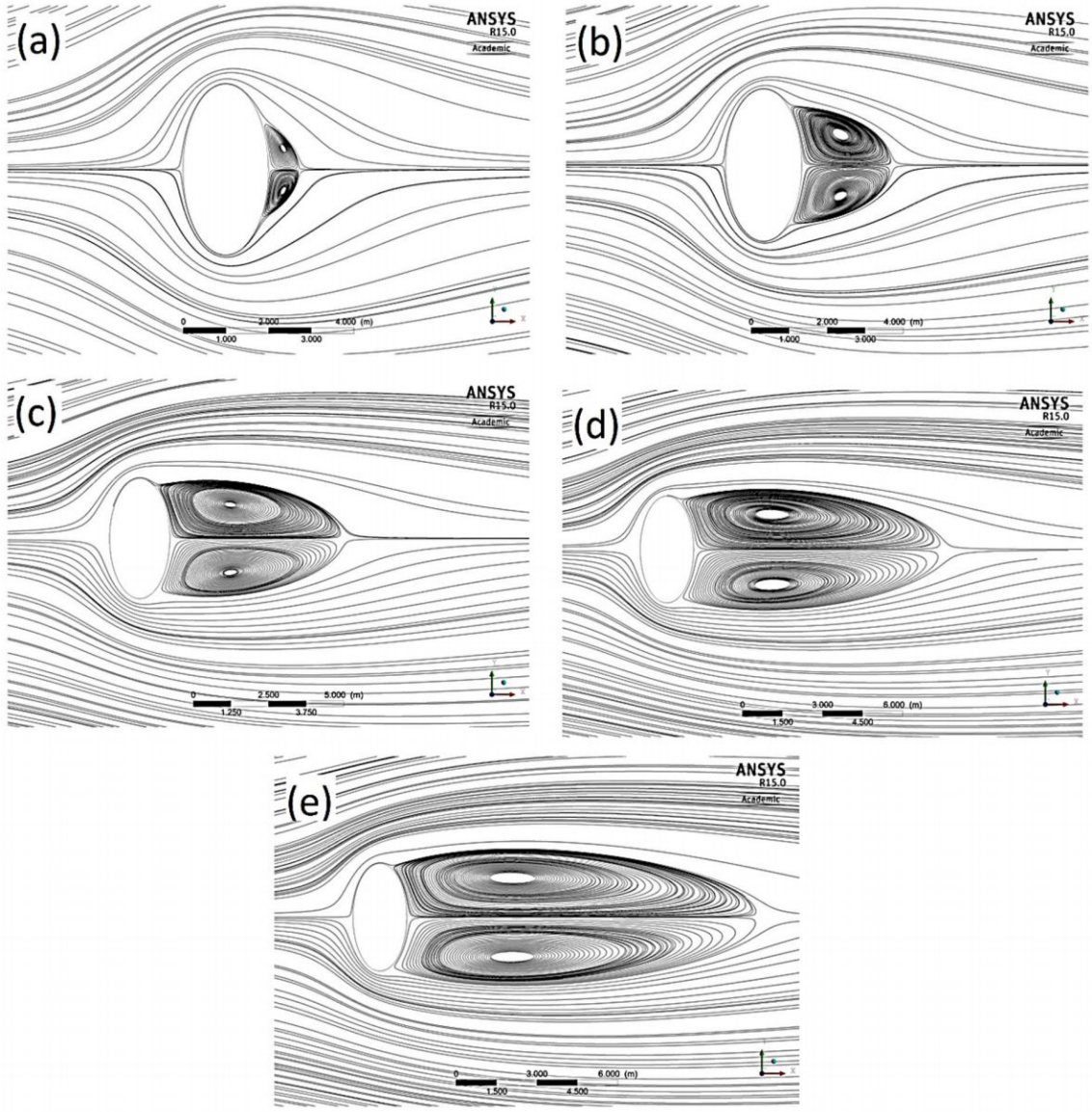

Figure 4.4: Streamlines for E=0.5, n=1 and (a) Re=5, (b) Re=10, (c) Re=20, (d) Re=30, (e) Re=40

In this case also, the wake size increases with increase in Reynolds number. For E = 0.5 (E < 1) it is observed that the body acts more like a bluff body with larger wakes in comparison to ellipse with E > 1. Due to bluff nature of the ellipse having E < 1, flow separation occurs early in the downstream direction due to a larger adverse pressure gradient than in a streamlined object.

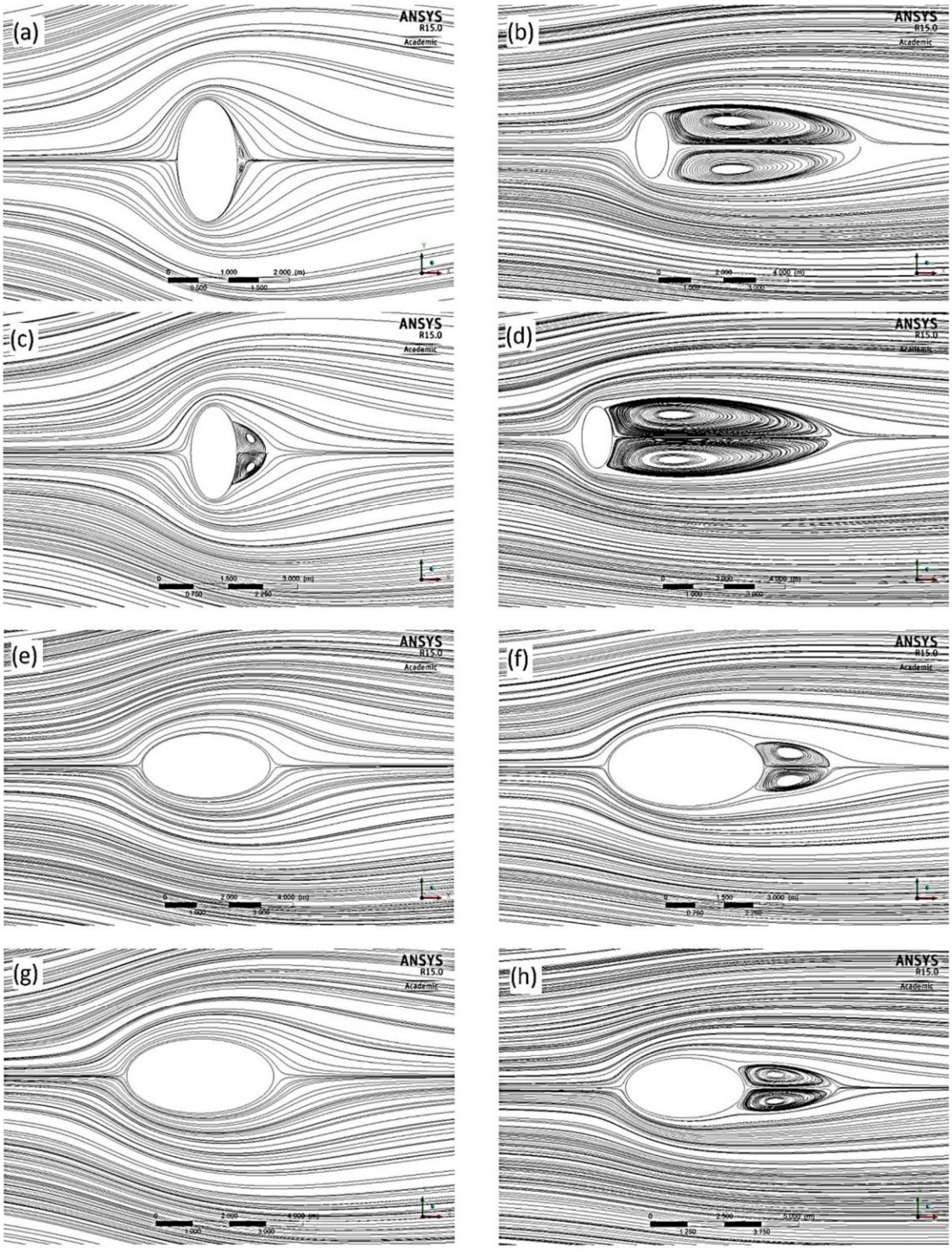

Fig 4.5: Streamlines for E=0.5 and (a) n=0.8, Re=5, (b) n=0.8, Re=40, (c) n=1.2, Re=5, (d) n=1.2, Re=40; for E=2 and (e) n=0.8, Re=5, (f) n=0.8, Re=40, (g) n=1.2, Re=5, (h) n=1.2, Re=40

It is observed that for same aspect ratio and Reynolds number, as power-law index is increased, the wake size also increases; this is more prominent at lower value of Reynolds number. This occurs due to early separation of the boundary layer from the body's surface in the case of low power-law index fluids because at lower Reynolds number, viscous forces are predominant, and the viscous forces vary with (velocity)^n. As the value of n is increased, viscous forces increase leading to faster dissipation of the velocity gradient in the boundary layer.

Table 4.3: Drag coefficient values (C_D) for E=2, 0.5; n=0.8, 1, 1.2; Re=5, 10, 20, 30, 40

Drag coefficient, C_D															
E=2															
n	Re=5			Re=10			Re=20			Re=30			Re=40		
	Pre.	Lit.	Error	Pre.	Lit.	Error	Pre.	Lit.	Error	Pre.	Lit.	Error	Pre.	Lit.	Error
0.8	4.6212	4.628	0.14%	3.0271	3.026	0.04%	2.0398	2.04	0.01%	1.6404	1.641	0.04%	1.4136	1.414	0.03%
1	4.2747	4.247	0.65%	2.9354	2.923	0.42%	2.0693	2.063	0.31%	1.7049	1.7	0.29%	1.4927	1.489	0.25%
1.2	3.948	3.948	0%	2.8339	2.834	0%	2.076	2.076	0%	1.7449	1.745	0.01%	1.5475	1.547	0.03%
E=0.5															
n	Re=5			Re=10			Re=20			Re=30			Re=40		
	Pre.	Lit.	Error	Pre.	Lit.	Error	Pre.	Lit.	Error	Pre.	Lit.	Error	Pre.	Lit.	Error
0.8	4.1051	4.101	0.01%	2.7753	2.775	0.01%	1.9857	1.986	0.02%	1.6747	1.675	0.02%	1.4981	1.498	0.01%
1	3.8448	3.828	0.44%	2.7284	2.72	0.31%	2.0249	2.02	0.24%	1.7315	1.728	0.20%	1.559	1.557	0.13%
1.2	3.6152	3.615	0.01%	2.6734	2.674	0.02%	2.0456	2.046	0.02%	1.7712	1.771	0.01%	1.6052	1.605	0.01%

Table 4.4: Pressure drag coefficient values (C_{DP}) for E=2, 0.5; n=0.8, 1, 1.2; Re=5, 10, 20, 30, 40

Pressure drag coefficient, C_{DP}															
E=2															
n	Re=5			Re=10			Re=20			Re=30			Re=40		
	Pre.	Lit.	Error	Pre.	Lit.	Error	Pre.	Lit.	Error	Pre.	Lit.	Error	Pre.	Lit.	Error
0.8	1.7925	1.794	0.08%	1.2633	1.262	0.10%	0.9343	0.934	0.03%	0.7989	0.799	0.00%	0.7211	0.721	0.01%
1	1.5755	1.56	0.99%	1.1609	1.16	0.08%	0.8949	0.889	0.63%	0.7825	0.778	0.57%	0.7163	0.7126	0.52%
1.2	1.3948	1.394	0.06%	1.0699	1.069	0.08%	0.8537	0.853	0.05%	0.7594	0.759	0.05%	0.7027	0.7023	0.06%
E=0.5															
n	Re=5			Re=10			Re=20			Re=30			Re=40		
	Pre.	Lit.	Error	Pre.	Lit.	Error	Pre.	Lit.	Error	Pre.	Lit.	Error	Pre.	Lit.	Error
0.8	2.9493	2.952	0.09%	2.0626	2.065	0.12%	1.551	1.553	0.13%	1.3528	1.354	0.09%	1.2391	1.24	0.07%
1	2.6455	2.617	1.09%	1.9425	1.925	0.91%	1.5144	1.504	0.69%	1.339	1.331	0.60%	1.2352	1.229	0.50%
1.2	2.3896	2.38	0.40%	1.8283	1.822	0.35%	1.4681	1.464	0.28%	1.3138	1.31	0.29%	1.2202	1.217	0.26%

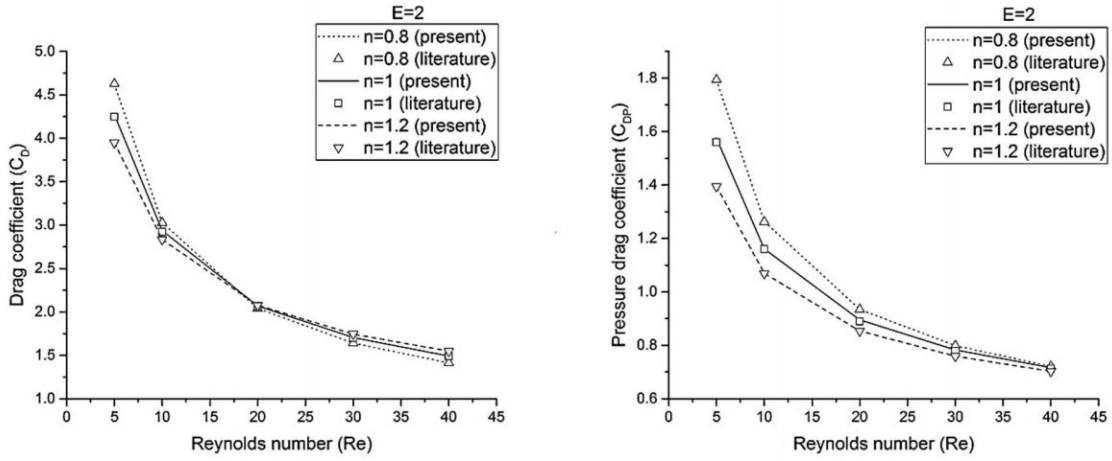

Figure 4.6: Plots of drag coefficient (C_D) and pressure drag coefficient (C_{DP}) for E=2; n=0.8, 1, 1.2; Re=5, 10, 20, 30, 40

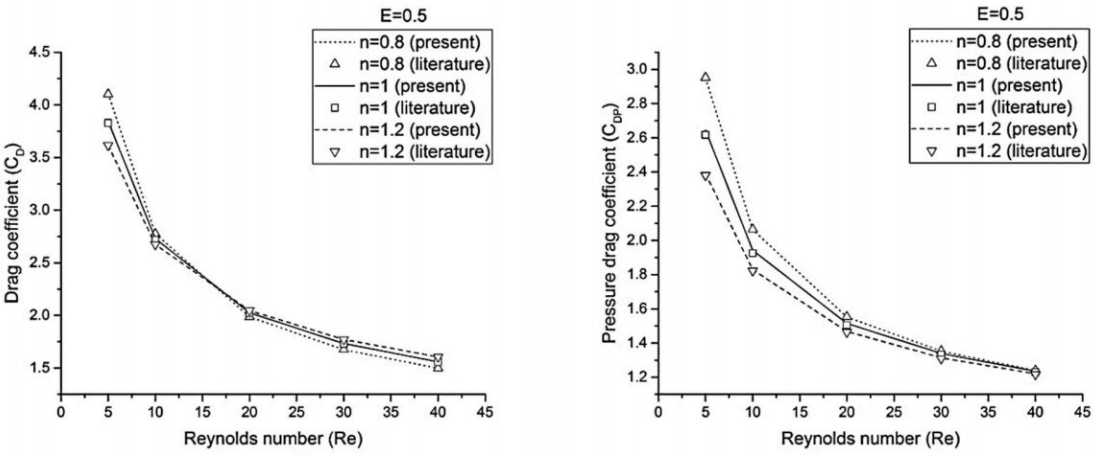

Figure 4.7: Plots of drag coefficient (C_D) and pressure drag coefficient (C_{DP}) for E=0.5; n=0.8, 1, 1.2; Re=5, 10, 20, 30, 40

Drag coefficient varies inversely with Reynolds number because the denominator in the expression of drag coefficient contains a v^2 term which rapidly increases with increase in Reynolds number. The drag coefficient is increased in shear-thinning ($n < 1$) fluids above its value in Newtonian media otherwise under identical conditions. As expected, shear-thickening ($n > 1$) fluids exhibit the opposite trend. However, the influence of power-law behavior index gradually diminishes with the increasing value of the Reynolds number. This can be rationalized by stating the fact that the viscous forces weaken as compared to the inertial forces with the increasing Reynolds number and, therefore, the power-law index is of little relevance under these conditions. We also see that at higher Reynolds number

flow, pressure drag coefficient forms a major part of the total drag coefficient. This occurs because at higher Reynolds number flow, larger wakes are formed which dissipate energy and increase the pressure difference between upstream and downstream positions.

4.3 Flow around a Rotating Circular Cylinder

Flow phenomena like drag and lift coefficient and streamlines were found out for a rotating circular cylinder and their dependence on Reynolds number (Re = 10, 40) and dimensionless rotational velocity (α = 2, 4, 6) was studied.

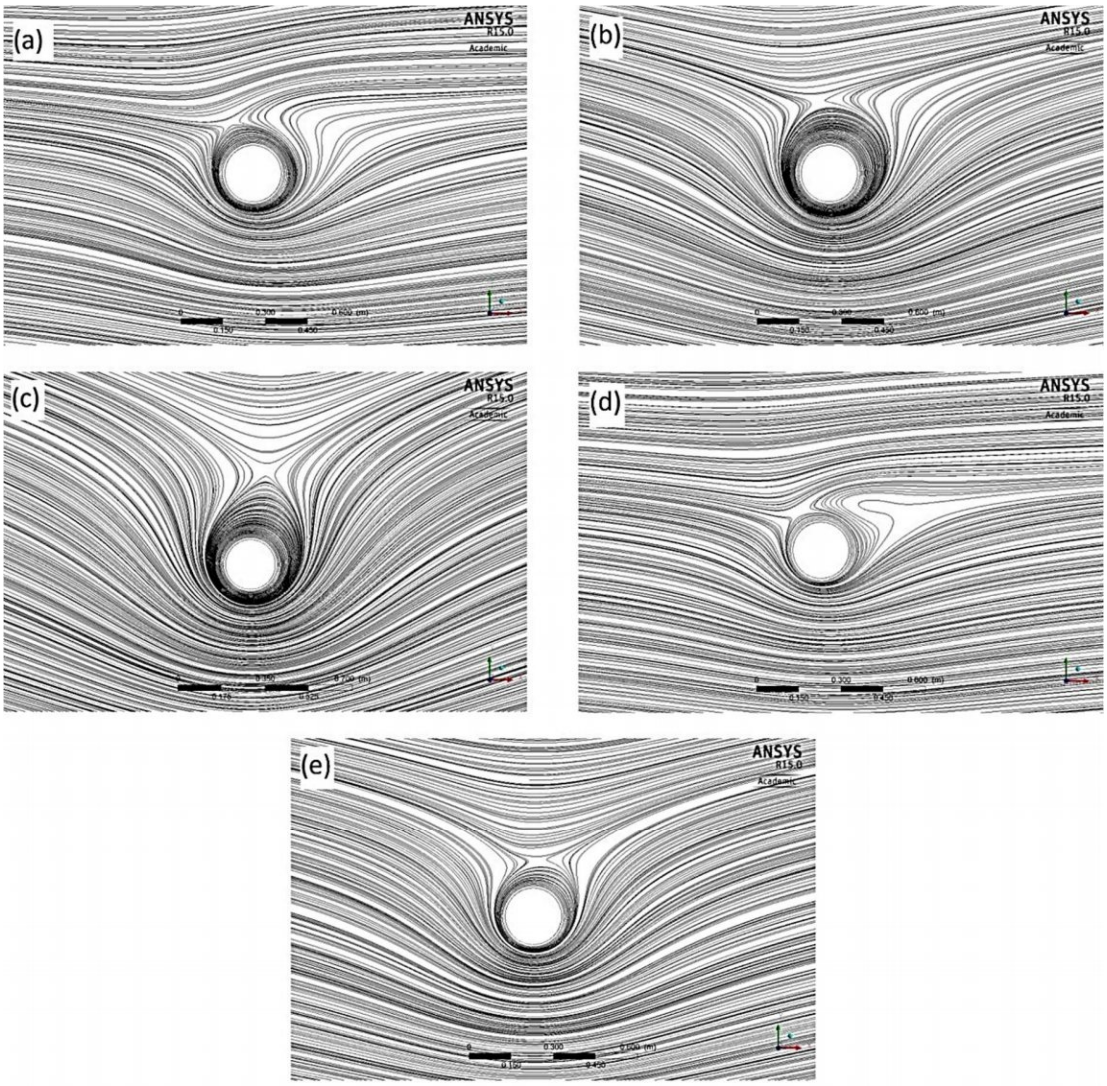

Figure 4.8: Streamlines for Re=10 and (a) α=2, (b) α=4, (c) α=6; for Re=40 and (d) α=2, (e) α=4

Table 4.5: Drag and Lift coefficients for Re=10, 40 and α=2, 4, 6 for a rotating circular cylinder

α	C_D		Error	C_L		Error
	Present	Literature		Present	Literature	
Rotating Circular Cylinder						
Re=10						
2	2.1335	2.134	0.02%	-5.956	-5.9608	0.08%
4	0.59058	0.5891	0.25%	-14.537	-14.5583	0.15%
6	-0.77801	-0.7747	0.43%	-28.623	-28.6372	0.05%
Re=40						
2	0.84774	0.8453	0.29%	-5.7091	-5.7205	0.20%
4	-0.1437	-0.144	0.21%	-16.101	-16.1329	0.20%
Rotating Domain, D'=1.2D						
Re=10						
2	1.9741	2.134	7.49%	-6.0019	-5.9608	0.69%
4	-0.25438	0.5891	143.18%	-14.23	-14.5583	2.26%
6	-3.2612	-0.7747	320.96%	-27.773	-28.6372	3.02%
Re=40						
2	0.66845	0.8453	20.92%	-4.5939	-5.7205	19.69%
4	-1.6211	-0.144	1025.76%	-9.6147	-16.1329	40.40%
Rotating Domain, D'=1.1D						
Re=10						
2	2.0903	2.134	2.05%	-5.9917	-5.9608	0.52%
4	0.38015	0.5891	35.47%	-14.584	-14.5583	0.18%
6	-1.3489	-0.7747	74.12%	-28.779	-28.6372	0.50%
Re=40						
2	0.76948	0.8453	8.97%	-5.5765	-5.7205	2.52%
4	-0.64932	-0.144	350.92%	-15.409	-16.1329	4.49%
Rotating Domain, D'=1.05D						
Re=10						
2	2.122	2.134	0.56%	-5.9681	-5.9608	0.12%
4	0.53823	0.5891	8.64%	-14.56	-14.5583	0.01%
6	-0.91297	-0.7747	17.85%	-28.682	-28.6372	0.16%
Re=40						
2	0.82431	0.8453	2.48%	-5.7039	-5.7205	0.29%
4	-0.2616	-0.144	81.67%	-16.069	-16.1329	0.40%
Rotating Domain, D'=1.02D						
Re=10						
2	2.1318	2.134	0.10%	-5.9592	-5.9608	0.03%
4	0.58057	0.5891	1.45%	-14.544	-14.5583	0.10%
6	-0.801	-0.7747	3.39%	-28.632	-28.6372	0.02%
Re=40						
2	0.8423	0.8453	0.35%	-5.7123	-5.7205	0.14%
4	-0.16273	-0.144	13.01%	-16.108	-16.1329	0.15%
Rotating Domain, D'=1.01D						
Re=10						
2	2.1325	2.134	0.07%	-5.9615	-5.9608	0.01%
4	0.58496	0.5891	0.70%	-14.555	-14.5583	0.02%
6	-0.79076	-0.7747	2.07%	-28.644	-28.6372	0.02%
Re=40						
2	0.84359	0.8453	0.20%	-5.717	-5.7205	0.06%
4	-0.15148	-0.144	5.19%	-16.123	-16.1329	0.06%

As the Reynolds number is increased we find that the drag coefficient decreases, this observation is similar to that of the stationary cylinder. We obtain a negative lift coefficient for all the cases due to anti-clockwise rotation of the cylinder. Higher lift coefficient is obtained for higher rotational speed. As the cylinder rotates, the top portion of the cylinder has fluid moving at a lower speed than the bottom portion of the cylinder. This causes a pressure difference between the two positions causing a lift force that is perpendicular to the free stream velocity. This observation is also known as the Magnus effect.

The calculated values give less than 1% error for a rotating circular cylinder without using the MRF model, because logically there is no need for using MRF for a circular cylinder because it does not deform the mesh while rotating. Second, we get best results (error < 5%) for D'=1.01D, i.e., a tight hugging rotating domain gives best results for a MRF problem. Also, we find out that as we increase the rotating domain size, the errors increase. A possible reason for this finding can be that a very thin region sticks to the rotating circular cylinder while the cylinder rotates, so rotating a bigger domain at the same constant rotating speed deviates from the ideal model.

This observation has been used to simulate a MRF model for a rotating elliptical cylinder, whose results are not available in the literature yet.

4.4 Flow around a Rotating Elliptical Cylinder

A MRF model simulation was done for a rotating elliptical cylinder and its flow phenomena like drag coefficient, lift coefficient and streamlines were reported for Re = 10, 40; α = 2, 4, 6; and different angles of attack θ = 0º, 30º, 60º, 90º, 120º, 150º

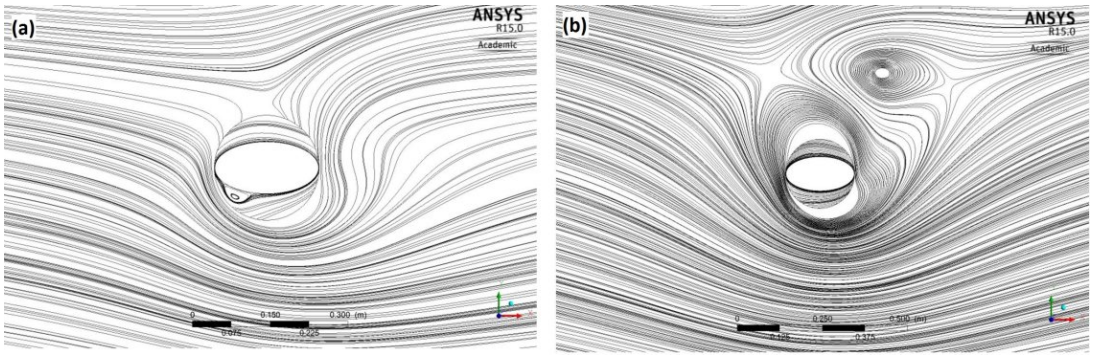

Figure 4.9: Streamlines for (a) Re=10, α=2; (b) Re=10, α=6 for a rotating elliptical cylinder

Table 4.6: Drag and lift coefficients for Re=10, 20, 30, 40; α=2, 4, 6; and θ = 0º, 30º, 60º, 90º, 120º, 150º

α	Re=10		Re=20		Re=30		Re=40	
	Cd	Cl	Cd	Cl	Cd	Cl	Cd	Cl
θ=0								
2	1.8662	-5.6651	1.0735	-4.7905	0.84173	-3.2799	0.75815	-2.2019
4	0.97077	-11.442	0.35947	-4.7052	0.58117	-2.2369	-	-
6	-0.71147	-13.758	-	-	-	-	-	-
θ=30								
2	0.67567	-5.5297	-0.30715	-5.9102	-0.78001	-6.0718	-1.0828	-6.1571
4	-2.58	-15.785	-4.3232	-16.665	-5.0129	-16.962	-5.4233	-17.281
6	-8.31	-31.251	-10.504	-30.113	-10.952	-29.274	-11.103	-29.061
θ=60								
2	0.54682	-3.2649	-0.37742	-3.1101	-0.76667	-2.9676	-0.9944	-2.8564
4	-4.0775	-8.9687	-5.1939	-7.5833	-5.5845	-6.6715	-5.7411	-6.0247
6	-11.425	-16.237	-12.2	-12.963	-12.464	-11.283	-12.34	-10.556
θ=90								
2	1.3897	-2.0874	0.51826	-1.6568	0.16908	-1.4426	-0.03585	-1.3585
4	-2.3064	-3.2642	-2.2159	-1.0285	-0.828	0.23811	-	-
6	-7.3	-3.2843	-	-	-	-	-	-
θ=120								
2	2.2505	-2.4291	1.3282	-1.6423	0.97187	-1.2263	0.79027	-1.0163
4	-0.17243	-2.2267	-0.48979	-0.59097	-	-	-	-
6	-2.6612	0.19114	-	-	-	-	-	-
θ=150								
2	2.5454	-3.8048	1.6959	-2.4627	1.4103	-1.7038	1.2729	-1.3661
4	1.3969	-4.3298	0.61908	-1.392	-	-	-	-
6	-0.04576	-1.3155	-	-	-	-	-	-

It was found that when the inclination angle of the elliptical cylinder was changed, different values of drag and lift coefficient were obtained. This is due to the static frozen-rotor approach incorporated by the MRF model. As the Reynolds number and rotating velocity were increased, it was found that some simulations failed to converge due to unsteady nature of the flow. With the same Reynolds number value, when dimensionless rotational speed was increased, it was found that more amount of fluid recirculated around the rotating cylinder, as was the case with the rotating circular cylinder. Smaller vortices were observed for lower rotational speed and larger vortices for higher rotational speed. Since MRF model is a steady-state approximation of the unsteady problem, we could not capture vortex shedding phenomena that would have actually formed for the rotating cylinder. Further, it is imperative to understand that the drag and lift values obtained by using this method are

only approximate values, implying that they cannot be fit into a general trend curve. However, these preliminary data are important for doing an unsteady-state simulation for the same problem by using a sliding mesh approach. The sliding mesh approach requires initial approximate velocity and pressure field for solving the unsteady-state problem, which has been obtained by the current research.

Chapter 5

Conclusions

The lid-driven square cavity problem has been solved first for Re=100, 400 and 1000. The streamlines have been reported and the reported velocity values have been found to be in good agreement with the literature values. After successfully solving the lid-driven square cavity problem, flow around an elliptical cylinder having an aspect ratio aspect ratio E=0.5, 2, for a fluid having power-law index n=0.8, 1, 1.2, for Re=5, 10, 20, 30, 40 has been numerically solved by using ANSYS Fluent (v. 15.0). Results obtained in the present work for different parameters such as drag coefficient, pressure drag coefficient and streamlines are found to be in good agreement with the literature values. From the present work it can be concluded that, as Reynolds number is increased, the drag coefficient values depend weakly on the power-law index due to inertial forces getting stronger as compared to viscous forces. Also, at higher Reynolds number, pressure drag coefficient forms a major part of the total drag coefficient.

It has also been found out that for a multiple reference frame (MRF) model, a tight hugging rotating domain gives best possible results with error less than 5% of the literature values. This observation has been used to simulate a MRF model for a rotating elliptical cylinder, whose results are not present in the literature yet. The streamlines of the rotating elliptical cylinder indicate that small vortices form at low rotational velocities and large vortices form at high rotational velocities for the same Reynolds number flow. It has further been observed that as rotational velocity increases, the recirculating fluid zone around the rotating cylinder increases in size. The velocity and pressure fields obtained from the current research can be used as initialization data for a transient sliding mesh approach for the same problem.

Scope for Further Research

The data obtained from the current research can be used as the starting point for a transient sliding mesh simulation of the same problem. Since this data is not available in the current literature, it would immensely benefit the scientific community if the said work is carried out in the near future.

References

[1] Masami Sato, Takaya Kobayashi, "A fundamental study of the flow past a circular cylinder using Abaqus/CFD", Mechanical Design & Analysis Corporation, SIMULIA Community Conference, 2012.

[2] B. M. Sumer, J. Fredsoe, "Hydrodynamics Around Cylindrical Structures", World Scientific, Singapore, 2006.

[3] Warren L. McCabe, Julian C. Smith, Peter Harriott, "Unit Operations of Chemical Engineering", Seventh Edition, International Edition 2005, McGraw-Hill Education (Asia), p. 159.

[4] I. Imai, "A new method of solving Oseen's equations and its applications to the flow past an inclined elliptic cylinder", Proceedings of the Royal Society A 224 (1954) 141-160.

[5] H. Hasimoto, "On the flow of a viscous fluid past an inclined elliptic cylinder at small Reynolds numbers", Journal of the Physical Society of Japan 8 (1958) 653-661.

[6] H. J. Lugt, H. J. Haussling, "Laminar flow past an abruptly accelerated elliptic cylinder at 45^{o} incidence", Journal of Fluid Mechanics 65 (1974) 711-734.

[7] N. A. Meller, "Viscous flow past an elliptic cylinder", Computational Mathematics and Mathematical Physics 18 (1978) 138-149.

[8] S. A. Johnson, M. C. Thompson, K. Hourigan, "Flow past elliptical cylinders at low Reynolds numbers", Proceedings of 14th Australasian Fluid Mechanics Conference, Adelaide, December 10-14, 2001, pp. 343-346.

[9] C. P. Jackson, "A finite-element study of the onset of vortex shedding in flow past variously shaped bodies", Journal of Fluid Mechanics 182 (1987) 23-45.

[10] Z. Faruquee, D. S.-K. Ting, A. Fartaja, R. M. Barron, R. Carreveau, "The effects of axis ratio on laminar fluid flow around an elliptical cylinder", International Journal of Heat and Fluid Flow 28 (2007) 1178-1189.

[11] D. Stack, H. R. Bravo, "Flow separation behind ellipses at Reynolds number less than 10", Applied Mathematical Modelling 33 (2009) 1633-1643.

[12] P. K. Rao, A. K. Sahu, R. P. Chhabra, "Flow of Newtonian and power-law fluids past an elliptical cylinder: a numerical study", Industrial & Engineering Chemistry Research 49 (2010) 6649-6661.

[13] V. A. Patel, "Flow around the impulsively started elliptic cylinder at various angles of attack", Computers & Fluids 9 (1981) 435-462.

[14] S. J. D. D'Alessio, S.C.R. Dennis, "A vorticity model for viscous flow past a cylinder", Computers & Fluids 23 (1994) 279-293.

[15] S. C. R. Dennis, P. J. S. Young, "Steady flow past an elliptic cylinder inclined to the stream", Journal of Engineering Mathematics 47 (2003) 101-120.

[16] P. Sivakumar, R. P. Bharti, R. P. Chhabra, "Steady flow of power-law fluids across an unconfined elliptical cylinder", Chemical Engineering Science 62 (2007) 1682-1702.

[17] R. P. Bharti, P. Sivakumar, R. P. Chhabra, "Forced convection heat transfer from an elliptical cylinder to power-law fluids", International Journal of Heat and Mass Transfer 51 (2008) 1838-1853.

[18] U. Ghia, K. N. Ghia, C. T. Shin, "High-Re Solutions for Incompressible Flow Using the Navier-Stokes Equations and a Multigrid Method", Journal of Computational Physics 48 (1982) 387-411.

[19] Saroj K. Panda, R. P. Chhabra, "Laminar flow of power-law fluids past a rotating cylinder", Journal of Non-Newtonian Fluid Mechanics 165 (2010) 1442-1461.

[20] Esam M. Alawadhi, "Numerical Simulation of Flow Past an Elliptical Cylinder Undergoing Rotationally Oscillating Motion", Journal of Fluids Engineering 137 (2015) 031106-031106-9.